PCCP

ROYAL SOCIETY OF CHEMISTRY

PAPER

View Article Online
View Journal | View Issue

Check for updates

Cite this: *Phys. Chem. Chem. Phys.*, 2023, **25**, 4649

Pt_{38} as a promising ethanol catalyst: a first principles study

Vagner Alexandre Rigo *[a] and Francesca Baletto [bc]

This first-principles study predicts Pt_{38} nanoparticles as a catalyst for ethanol reactions. Starting from the adsorption properties, we shed light on the effectiveness of Pt-based nanoclusters as ethanol catalysts. First, the ethanol adsorption on Pt_{38} shows that the most stable site positions the molecule with the oxygen anchored on top of an edge, whereas CH_3 is oriented towards the facet and the molecule remains in *trans*-symmetry. The ethanol–oxygen adsorbed on top of a facet Pt-atom offers the least stable configuration and the longer Pt–O distance (2.318 Å), while the shorter Pt–O distance (2.237 Å) is found when ethanol is on top of an edge site and the molecule is vertically oriented with Gauche symmetry. A shorter Pt–O distance correlates with higher radial breathing of the nanoparticle after ethanol adsorption. Atomic charge redistribution is calculated on all the considered systems and cases. In any event, we show that the Pt-anchor receives a charge, whilst oxygen–ethanol donates electrons. Orbital analysis shows that Pt-anchors and ethanol–oxygen atoms primarily exchange p-charge. Energy barriers associated with the ethanol bond cleavage show that the C–C bond break is slightly more favourable on Pt_{38} than on an extended Pt(111). In addition, we find that the cleavage of the hydroxyl O–H ethanol bond shows a higher energy barrier while the removal of an H-atom from the CH_3 group is easier. These three facts indicate that the Pt_{38} nanoparticle enhances ethanol catalysis and hence is a good candidate for ethanol-based fuel cells.

Received 16th September 2022,
Accepted 6th January 2023

DOI: 10.1039/d2cp04323h

rsc.li/pccp

Published on 09 January 2023. Downloaded on 4/7/2026 5:10:41 AM.

1 Introduction

Global warming[1,2] and the establishment of environmental targets[2] have driven attention towards newer and cleaner energy sources. In this regard, the progressive adoption of renewable energy sources could help reduce CO_2 emissions and help manage environmental pollution, but some practical issues remain, such as scale, cost, and efficiency associated with clean energy sources.[3–6]

Ethanol, a plant-based fuel, represents a renewable alternative to replace fossil fuels. It is non-toxic and can be easily obtained from organic materials.[6,7] A simple but central physical property of ethanol is that it remains liquid at ambient temperatures; so, the substitution of fossil fuels with ethanol could be implemented with minimal modifications to today's distribution networks.[6] Additionally, the global prices of ethanol as a commodity have been gradually reduced over the past decades, achieving values that are competitive if not lower than gasoline.[7]

The conversion of ethanol into electricity represents a step forward in the worldwide fight to reduce CO_2 emissions. In efficient ethanol-based fuel cells (EBFCs), electricity is produced from the chemical decomposition of ethanol molecules.[8] EBFCs can offer the possibility to increase the energy efficiency of transport vehicles.[6,8] Specifically, Pt-based nanocatalysts constitute efficient compounds to activate ethanol on anodes of EBFCs. However, the total charge per ethanol molecule obtained using Pt-based surfaces on anodes reaches roughly 1/3 of the feasible theoretical maximum.[8–11] This typically occurs because the catalytic process terminates mainly with the formation of acetaldehyde (CH_3 CHO) and acetic acid (CH_3 COOH), which hinders the formation of the CO_2 molecules required for the total oxidation process.[8,10,12]

Pt-nanoparticles (Pt-NPs) display a variety of facets and surface site coordination compared to extended surfaces.[13–19] Recent findings show that these topological details could enhance the catalyst activity of Pt-NPs regarding the activation of organic compounds, as opposed to surfaces.[17] This is supported by experimental results showing that ethanol catalysis increases when small-size Pt-nanoparticles are employed.[11,20] Based on this, Pt-NPs represent an attractive possibility for increasing the efficiency of EBFCs.

This work predicts the activity of 38-atoms Pt-NPs as a catalyst for key ethanol reactions by means of first-principles calculations. We carefully map the adsorption of ethanol on Pt_{38}, and we carry on energetic, structural, and charge analyses.

[a] *Department of Natural Sciences, Universidade Tecnológica Federal do Paraná (UTFPR), Cornélio Procópio, 86300-000, Brazil. E-mail: vagnerrigo@utfpr.edu.br; Tel: +55 43 3133 3917*
[b] *Physics Department, University of Milan, Via Celoria 16, 20133, Italy*
[c] *Physics Department, King's College London, Strand WC2R 2LS, UK*

Published on 09 January 2023. Downloaded on 4/7/2026 5:10:41 AM.

Furthermore, we study some ethanol dissociation processes. Our results show interesting features with respect to (111) Pt-surfaces. Our findings indicate that Pt-NPs favour the cleavage of the C–C bond and the CH_3 radical, but tend to prevent hydroxyl cleavage. Such information clearly suggests that Pt_{38} is a good candidate for enhancing ethanol catalysis within EBFCs.

2 Materials and methods

We employ the spin-polarized total-energy density functional theory (DFT) calculations[21,22] processed through the Quantum ESPRESSO suite.[23,24] The generalized gradient approximation of Perdew, Burke, and Ernzerhof (PBE)[25] is adopted to describe the exchange-correlation interactions. The atomistic systems contain charge-neutral Pt, O, C, and H atoms, whose atomic numbers are 78, 8, 6, and 1, respectively. Ultrasoft pseudopotentials are used to describe core–valence electron interactions,[26] and the electronic distribution of valence electrons $5d^9 6s^1 6p^0$, $2s^2 2p^4$, $2s^2 2p^2$, and $1s^1$ is considered for Pt, O, C, and H pseudopotentials, respectively. A plane-wave energy cutoff of 25 Ry and Gamma-point calculations are used for Brillouin-zone sampling, and a vacuum slab of at least 11 Å is adopted. The van der Waals dispersion interaction is described using the Grimme formulation (PBE + D3).[27] All geometries are optimized using the Broyden–Fletcher–Goldfarb–Shanno (BFGS) method[23,24,28,29] until forces on atoms are lower than 1×10^{-3} Ry $Bohr^{-1}$ and the total energy difference between two consecutive self-consistent interactions changes less than 1×10^{-4} Ry. The maximum displacement of atoms between two minimization steps was set as 0.8 Bohr along the minimization process. The atomic charges are obtained through projection on atomic orbitals.[30]

We consider a 38-atom truncated octahedron Pt-nanoparticle (Pt_{38}). This structure is an Archimedean solid that obeys the Wulff theorem of shape stability of crystals.[15,31] It is obtained by cutting a piece of a face-centered cubic Pt-bulk structure. According to the Wulff theorem, the further growth of the (100) and (111) facets respects the ratio between these surface energies. The final Pt_{38} structure does not present a central atom. For details about the shape and structure of nanoparticles, ref. 31 can be referred to. The rationale of this nanoparticle is twofold, delimited by both (100) and (111) types of facets, connected at the corners and edges by low coordination Pt-atoms. So, Pt_{38} offers a greater variety of surface sites to evaluate ethanol adsorption if compared to other intermediate-size structures, as the (111) delimited Pt_{55}.[15,16,32] Furthermore, compared to smaller and larger samples, intermediate-size Pt nanoparticles exhibit favourable adsorption and catalytic properties for ethanol molecules,[12,20,33–36] with similar effects reported for water dissociation on Pt_{38} nanoparticles.[37] Based on this, Pt_{38} represents a substrate for ethanol catalysis that deserves more attention. Studies regarding the adsorption of ethanol molecules on Pt-extended surfaces[38–40] and nanoparticles[16,19,41] confirmed that the adsorption of the ethanol–oxygen atom on top of a surface Pt-atom is energetically favourable, with adsorption on the low coordinated vertex sites representing relevant sites among nanoparticle from the energetic point of view. The orientation of the ethanol ethyl tail also plays a role, where configurations with the C–C bond oriented towards the Pt-surface, approaching the H-atoms in CH_2 and CH_3 to the top of Pt atoms, are the most stable structures. Since these conclusions are confirmed for some different sizes and specific shapes of nanoparticles,[16,19,41] here we concentrated on evaluating the most relevant adsorption possibilities on Pt_{38} that keeps the ethanol oxygen atom on top of a Pt-atom. Both vertex and facet Pt-atoms are considered to adsorb the ethanol oxygen and the orientation of the C–C ethanol bond is evaluated along the edge and facet Pt-atoms and vertically oriented when the ethanol molecule presents the gauche symmetry. The entire optimization process was carried out for all proposed adsorbing configurations, and the actual results correspond to the optimized configurations. Fig. 1 presents the obtained adsorption sites on Pt_{38} following the full geometry optimization process. The adsorption energy, E_{ads}, of ethanol on a nanoparticle is

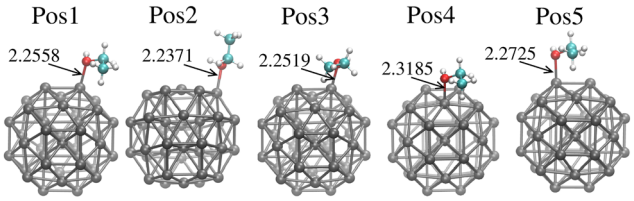

Fig. 1 Ethanol adsorption sites on Pt_{38} nanoparticles. Each position shows the distance between ethanol–oxygen and Pt-anchor in Å units. Grey, cyan, white and red balls represent the Pt, C, H, and O atoms, respectively.

$$E_{ads} = E_{Sys} - E_{Pt_{38}} - E_{Mol}, \quad (1)$$

where E_{Sys} is the total energy of the full system relaxed after the adsorption of ethanol on a certain site. $E_{Pt_{38}}$ and E_{Mol} are the total energies of the pristine Pt_{38}, and the molecule in the gas phase, respectively.

The Nudge Elastic Band method[23,24] with the Climbing Image procedure was used to obtain the transition states. The initial and final images were kept fixed, and the images were connected by springs defined by a variable spring constant between 0.3 and 0.2 a.u. The path is optimized using the Broyden Second method[42,43] until the intensity of the force orthogonal to the path was lower than 0.1 eV $Å^{-1}$. Since the ethanol–Pt_{38} interaction occurs mainly through enthalpy-driven van der Waals interactions, zero point energy and temperature were not considered.

Rearrangements of the Pt_{38} structure after molecular adsorption are evaluated from the cluster's radial breathing. This quantity accounts for the variation of the radial position r^i of the atom i with respect to the centre of mass of the nanoparticle, before and after the adsorption.

$$\Delta r^i = r^i_{Sys} - r^i_{Pt_{38}}, \quad (2)$$

where $r^i_{Pt_{38}}$ and r^i_{Sys} stand for the radial position of the atom i before and after adsorption, respectively.

 This journal is © the Owner Societies 2023

Published on 09 January 2023. Downloaded on 4/7/2026 5:10:41 AM.

The charge distribution is evaluated based on the charge difference for each atom i before and after EtOH adsorption,

$$\Delta q^{i} = q^{i}_{Sys} - q^{i}_{Pri}, \quad (3)$$

where q^{i}_{Sys} and q^{i}_{Pri} are the charges of the atom i, before and after the adsorption, respectively.

3 Results

Fig. 1 shows the evaluated ethanol adsorption sites on Pt_{38}. The different sites account for the most relevant chemical aspects of the molecule–Pt_{38} interaction. We interpret our results by reporting both the relative position of oxygen and the orientation of the CH_3 group. Generally speaking, the adsorption of oxygen–ethanol on top of edge sites shortens the Pt–O distance (d_{Pt-O}), while d_{Pt-O} is longer when the oxygen lies on top of a facet Pt-atom. Specifically, Position 2 (Pos2) shows the molecule on the Gauche symmetry on top of an edge-Pt site, with the CH_3-group far from the Pt_{38} surface. This site is characterised by the shortest distance between the oxygen–ethanol and surface-Pt atoms (2.2371 Å), between the evaluated sites. The positions Pos1, Pos3, Pos4 and Pos5 show the *trans*-ethanol falling on the surface, with the CH_3 group close to a surface Pt-atom. Pos4 presents the oxygen–ethanol adsorbed on the centre of a facet and exhibits the longer Pt–O distance (2.3185 Å), with the oxygen–ethanol on top of a facet Pt-atom.

Table 1 reports the adsorption energies and the intra-ethanol bond lengths upon adsorption. In general, the oxygen anchored on an edge Pt-atom represents the most stable position, but the orientation of the ethyl tail also interferes. In detail, Pos3 is the most stable site, followed by Pos5, while each presents the oxygen on top of an edge site and the ethyl tail toward the facet. Pos4 presents the higher E_{ads}. Interestingly, the Gauche symmetry, where ethanol is adsorbed on the edge, as in the Pos2, is slightly higher in energy compared to other sites with the oxygen on the top edge. Notably, Pos2 presents the longest d_{C-C} and d_{O-H}, but the lowest d_{Pt-O} between the evaluated sites. The most stable site, Pos3, presents the longer d_{C-O}. Together, these variations in bond length could give clues to the charge transfer between atoms, thereby helping to identify catalytic routes.

Fig. 2 represents the radial breathing of Pt_{38}, according to eqn (2). The results show that the adsorption site and the ethanol orientation and symmetry affect the overall geometry, as expected. For every considered site, the Pt-anchor is pushed up upon adsorption. Among these, the Pt_{38} nanostructure undergoes

Table 1 Adsorption energies, using eqn (1), and intramolecular bond distances of ethanol molecule upon adsorption on Pt_{38}

Ads. site	E_{ads} (eV)	d_{C-O} (Å)	d_{C-C} (Å)	d_{Pt-O} (Å)	d_{O-H} (Å)
Pos1	−0.796	1.4761	1.5085	2.2558	0.9788
Pos2	−0.766	1.4761	1.5126	2.2370	0.9835
Pos3	−0.835	1.4795	1.5085	2.2519	0.9789
Pos4	−0.648	1.4702	1.5086	2.3185	0.9822
Pos5	−0.820	1.4788	1.5081	2.2725	0.9783

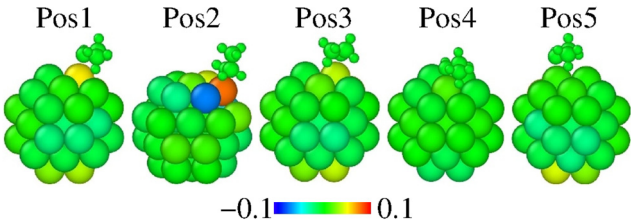

Fig. 2 Radial breathing of Pt_{38} atoms of evaluated adsorption positions according to eqn (3). The scale bar is in Å units. The ethanol colors are meaningful and the molecule is shown in each adsorption position for reference.

fewer rearrangements when the molecule is adsorbed on the facet centre, as in a Pos4 site. The most significant modifications occur on Pos2, where the ethanol with Gauche symmetry is on top of an edge site. This information seems to indicate the strengthening of the Pt–O bond with the shortening of the Pt–O distance and a larger charge transfer.

Fig. 3 presents the density of states (DOS) for the pristine Pt_{38} and ethanol molecules, and the projected density of states (PDOS) on Pt_{38} and the ethanol upon molecule adsorption on the most stable Pos3 configuration. We observed that the energy levels for Pt_{38} before and after ethanol adsorption spread between ∼−9 and ∼−9 eV. Before adsorption, the empty ethanol states are localized within 2–3 eV, while the occupied states are localized within ∼−3 and ∼−9 eV. Upon adsorption, the formation of the oxygen–Pt bond and charge transfer take place, and the unoccupied ethanol levels are shifted to ∼−3 to 8 eV. Such data indicate that part of the ethanol valence charge is transferred to Pt_{38} and that the molecule becomes positively charged. The valence band maximum for the pristine and adsorbed ethanol molecule is at the same position, but the narrower peak for the pristine, compared to the adsorbed one, indicates hybridization takes place after adsorption. Furthermore, the peak at ∼−4.5 eV, present for the Pt_{38} and the adsorbed ethanol, reveals the hybridization due to bond formation between the adsorbed molecule and the nanoparticle.

Fig. 4 presents the PDOSs for some orbitals of the Pt-anchor atom prior to and upon ethanol adsorption onto Pt_{38}. Most of the occupied 6 s states of Pt-anchor reduce their intensity for Pos3 geometry, compared to the pristine nanoparticle, especially close to the Fermi level. The peak reduction of occupied states

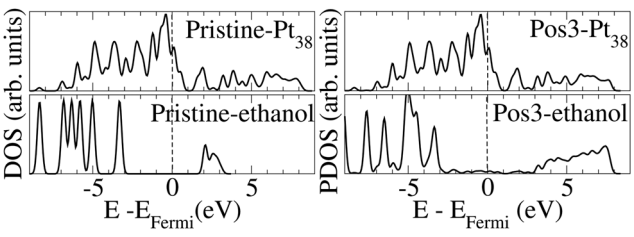

Fig. 3 DOSs for Pt_{38} and ethanol molecules in the pristine configurations and PDOs of Pt_{38} and molecules upon ethanol adsorption onto Pos3 configuration. The data correspond to the optimized configurations, and the Fermi level is at zero energy, indicated by the vertical dashed line.

Published on 09 January 2023. Downloaded on 4/7/2026 5:10:41 AM.

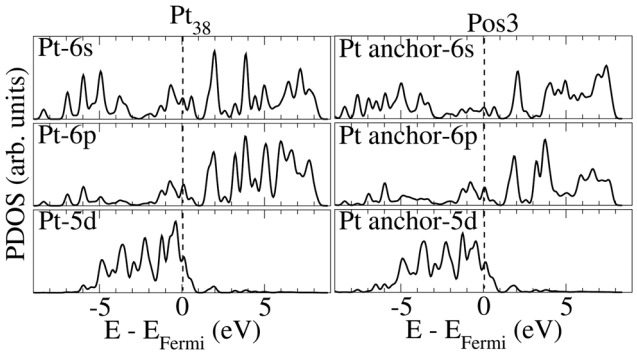

Fig. 4 PDOSs for the 6 s, 6 p, and 5 d orbitals for the surface Pt-anchor atom before (left) and after (right) ethanol adsorption onto Pt_{38} on Pos3 configuration. The data correspond to the optimized configurations, and the Fermi level is at zero energy, as indicated by the vertical dashed line.

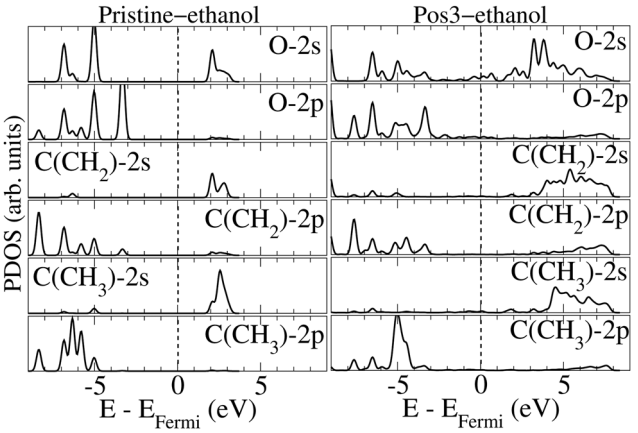

Fig. 5 PDOSs for the 2 s and 2 p orbitals of oxygen and the carbon atoms of CH_2 and CH_3 ethanol radicals before (left) and after (right) ethanol adsorption onto Pt_{38} on the Pos3 configuration. The data correspond to the optimized configurations and the Fermi level is at zero energy, as indicated by the vertical dashed line.

could indicate that the 6 s orbital acts as an electron donor. A similar effect is verified for the 5 d energy levels close to the Fermi level. On the other hand, the occupied 6 p orbitals between ~ -5 and ~ -7 eV increase.

Fig. 5 presents the PDOSs of selected orbitals for the oxygen and carbon atoms in the ethanol molecule prior to and after adsorption on Pos3 geometry. The rsults reveal that the 2 s empty oxygen levels, concentrated between 3 and 4 eV before adsorption, spread from the Fermi level up to 8 eV when adsorbed. The introduction of peaks near 1 eV and 2 eV reveal that oxygen 2 s and Pt-anchor 6 s hybridization occurs. A similar situation is verified for the occupied levels, where a broad spread occurs upon adsorption for most levels. The occupied levels for the oxygen-2 p orbital present a broadening of the levels between ~ -7 eV and ~ -4.5 eV upon adsorption, but the introduction of some peaks, like ones at ~ -4.5 eV and ~ -0.5 eV, also indicates hybridization with Pt-anchor. Notably, the occupied 2 s and 2 p peaks related to oxygen present a reduction in intensity, whereas the empty peaks seem to enlarge, suggesting a charge donation upon ethanol adsorption. In the same direction, alterations could be found on levels related to 2 s and 2 p orbitals of ethanol carbon atoms as well. Upon adsorption, the 2 s and 2 p orbitals of carbon atom in CH_2 radical increase below the Fermi level but diminish for the empty states, compared to the pristine-ethanol. In contrast, the 2 p orbital of the carbon atom in CH_3 close to ~ -5.0 eV shows a notable intensity increase.

Fig. 6 presents the total and orbital charge redistribution upon ethanol adsorption, (Δq^i), according to eqn (3). In any event, after the ethanol adsorption, a charge transference occurs. Regarding total charge, the Pt-anchor receives charge while the O-atom acts as a donor, in line with the results of Verga *et al.*[19] Other details of note emerge from Fig. 6. First, the Pt-anchor located on an edge site receives more charge, compared to a facet adsorption site, like Pos4. This indicates a stronger chemical interaction when the oxygen is on top of an edge site. This observation aligns with the greater Pt–O bond distance and weaker E_{ads} of Pos4. Second, the position of the CH_3 on the Pt-NP seems to affect the charge redistribution.

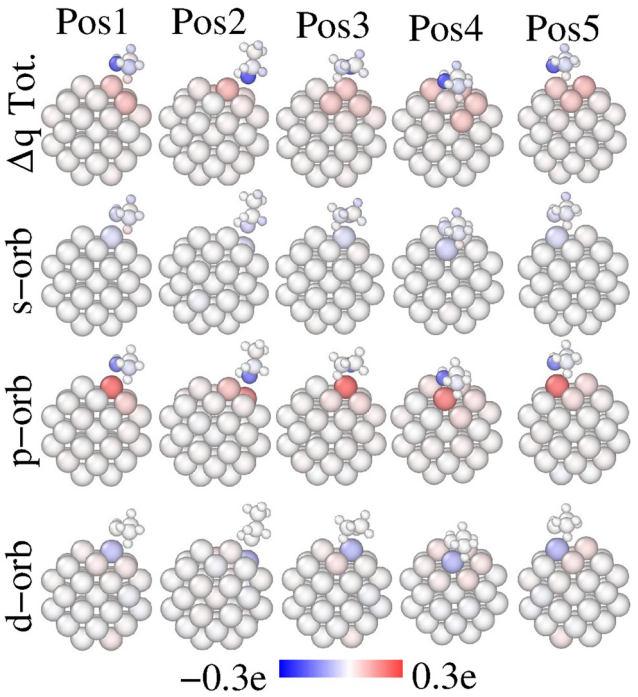

Fig. 6 Charge redistribution upon ethanol adsorption for the evaluated sites, according to eqn (2). The total, s, p and d charge redistributions are shown in the first, second, third and fourth rows, respectively. Red color accounts for a charge gain of the atom upon ethanol adsorption, whereas, blue indicates a charge loss upon adsorption.

In this regard, the Pt-anchor receives more charge if ethanol is on Pos3 and Pos5, which presents CH_3 on top of a facet. Furthermore, a charge gain occurs in all H-atoms of the CH_3 group nearby a Pt-atom. This indicates that the H-atoms within the CH_3 group are affected in different ways due to the proximity of Pt-atoms. Interestingly, the C-atom within the

 This journal is © the Owner Societies 2023

Published on 09 January 2023. Downloaded on 4/7/2026 5:10:41 AM.

CH_3 group donates charge upon adsorption only on the Pos2 site, but gains charge in all other positions. This contrasting charge transfer pattern on the CH_3 group indicates that different adsorption sites could affect the ethanol bond cleavage differently. Notably, experiments under reactive conditions using sum frequency generation (SFG) vibrational spectroscopy suggested that the ethanol C–C bond is more perpendicular to the Pt surface in the gas phase, while the bond is approximately parallel to the surface in the liquid phase.[44] Furthermore, the authors showed that the selectivity toward total oxidation toward CO_2 is approximately 42% greater in the gas phase, whereas the selectivity toward incomplete oxidation toward acetaldehyde is almost 2% lower in the gas phase compared to the liquid one. Such pieces of information connect with the longest C–C bond obtained for the Pos2 adsorption site obtained in the present work (Table 1), indicating that this position may favor the selectivity toward C–C cleaving. The orbital charge analysis clarifies that the Pt-anchor receives a p-charge but donates s- and d-charges in all evaluated configurations. This fact implies a s → p and d → p charge transfer upon ethanol adsorption. In any event, we show that oxygen–ethanol losses primarily p-charge independently of the adsorption site feature. These findings are consistent with the DOS and PDOS analyses presented in Fig. 3 and 5.

To better characterize the ethanol–nanoparticle energetics, we estimate the energy activation barriers involved in the displacement of the molecule along the Pt_{38} surface. This information is relevant for evaluating the diffusion of molecules on nanoparticles and could be useful for deriving an adjusted force field. The displacement of the ethanol molecule along with two neighbour edge sites and between an edge and a facet site was considered. Fig. 7 shows the obtained barriers. These results demonstrate that activation energies are similar along both paths (about 0.42 eV), and that at equilibrium and ambient temperatures, the Boltzmann weights related to the endpoint positions give the probability that finding the molecule on Pos1 is approximately 252.1 times greater than for Pos4. On the other hand, the probability of finding the ethanol on Pos5 is approximately 2.5 times that of Pos1. These results indicate the far greater likelihood of finding the ethanol adsorbed with oxygen on top of an edge site in a rarefied atmosphere at ambient temperature, as the orientation of the ethyl towards the facet centre also plays a role in stabilizing the system.

Since ethanol is a complex molecule, there are a number of different chemical routes to dissociate it. In most of the cases, the ethanol oxidation reaction terminates with the formation of acetic acid and acetaldehyde. This typically occurs when reactions are catalyzed by an extended Pt-surface.[8–11,45] However, the promotion of the C–C bond cleavage towards CO_2 production as a final outcome of the reaction could be enhanced using nanocatalysts. Considering that the straight, one-step, C–C bond cleavage of ethanol molecules is highly unlikely due to the high energy activation barrier, as shown on Pt-surfaces,[45] here, we focus our attention on other key reactions leading to ethanol dissociation on Pt_{38}.

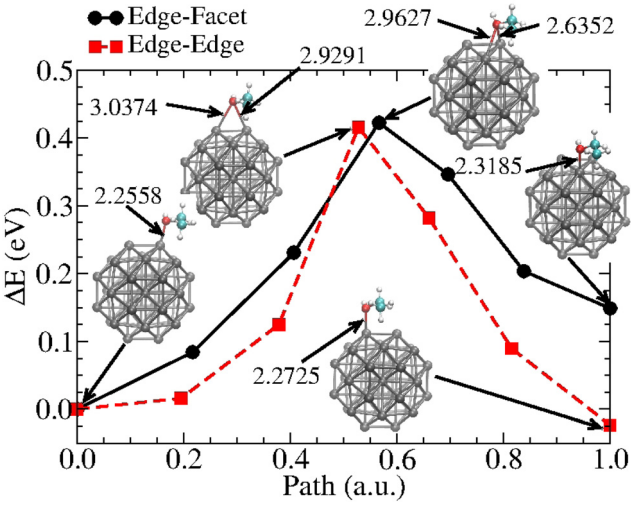

Fig. 7 Energy activation barriers for the diffusion of an ethanol molecule from an edge (Pos1) to a neighbor facet (Pos4)-dark circled dots- and from Pos1 to an edge surface site (Pos5)-red squared dots. The geometries of the initial and final configurations and the transition states are presented as insets, and the distances are in Å.

Fig. 8 and Table 2 show the energy profiles related to ethanol dissociation. Selected results from the literature which consider extended Pt-surfaces are reported in Table 2 for easier comparison. The findings show that reactions starting from the ethanol H-atoms bonded to carbon atoms are favoured on Pt_{38}. On the other hand, the cleavage of the hydroxyl O–H bond has a larger barrier (1.25 eV), compared to the extended (111) Pt-surface (0.88 eV). This represents an increase of approximately 42% in the energy cost associated with the O–H bond cleavage on the Pt-nanoparticles, compared to the surface. Furthermore, such an increment suggested that this reaction is unlikely to occur on Pt_{38}. Other reactions toward the acetaldehyde (CH_3 CHO), which requires hydroxyl cleavage, are unfavourable on Pt_{38} compared to Pt(111). However, the ethanol C–C bond cleavage is more favourable on Pt_{38} than on the

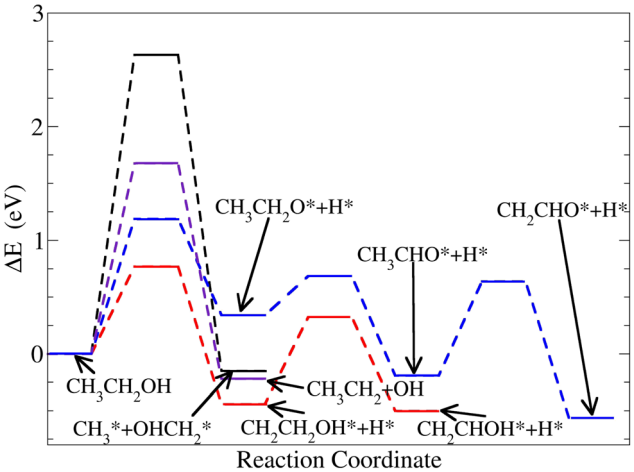

Fig. 8 Energy profiles of the four alternative reaction pathways with an adsorbed ethanol starting on Pos3 on Pt_{38}.

Published on 09 January 2023. Downloaded on 4/7/2026 5:10:41 AM.

Table 2 Energy barriers for ethanol dissociation on Pt_{38} for evaluated energy pathways. The central column shows the data obtained in the present study and the right column presents data for ethanol dissociation on Pt-extended surfaces from the literature

Reaction	ΔE (eV)	ΔE (eV)
CH_3CH_2 OH → CH_3 +CH_2 OH	2.63	2.98 Pt(111)[45]
CH_3CH_2 OH → CH_2CH_2 OH + H	0.77	0.89 Pt(111)[45]
CH_3CH_2 OH → CH_3CH_2 O + H	1.25	0.88 Pt(111)[45]
CH_3CH_2 OH → CH_3CH_2 +OH	1.67	
CH_3CH_2 O → CH_3 CHO + H	0.38	
CH_3 CHO → CH_2 CHO + H	1.25	1.12 Pt(111)[45]
CH_2CH_2 OH → CH_2 CHOH + H	0.76	

(111) surface. Although the straight C–C bond cleavage is unlikely, the reduction of approximately 13% in the activation energy indicates a favourable C–C cleavage on Pt-nanoparticles. These results are aligned with the enhanced ethanol oxidation reaction reported on (100) terminated cubic nanoparticles, compared to (110), (111), (211), and (311) facets, as presented in a recent experimental study conducted by Wang *et al.*[46] The energy activation barriers are reduced on Pt_{38} when the ethanol dissociation begins with the removal of an H-atom from the CH_3 group. This information is consistent with the charge gain of the H-atom on CH_3 located close to the nanoparticle surface, as in Pos1 of Fig. 6. The improvement in ethanol oxidation reaction on Pt_{38}, with regard to the extended (111) Pt-surface, is consistent with experimental studies with smaller-size Pt-nanoparticles.[47]

4 Conclusions

One of the greatest challenges to increase the efficiency of EBFCs is finding a catalyst which can surpass the formation of acetaldehyde (CH_3 CHO), hindering the formation of acetic acid (CH_3 COOH). Indeed, CH_3 CHO and CH_3 COOH are the most common products during the dissociation of ethanol on extended Pt surfaces. Unfortunately, they are not the most desirable products,[8,10] and better catalysts are needed. Anyone can easily notice that both products have the CH_3 radical in their structure. Here we find that Pt-truncated octahedra as small as 38 atoms could solve the issue. Indeed, by first-principles calculations, we show that the activation of the CH_3 group by removing H-atoms is more favourable on a Pt_{38} nanoparticle than on a flat, extended (111) Pt-surface, as shown in Fig. 7 and Table 2. Our results indicate that Pt-nanoclusters could be employed to increase the efficiency of EBFCs because they facilitate mechanisms toward the complete ethanol oxidation reaction.

Author contributions

The authors contributed equally to this work. All authors have given approval to the final version of the manuscript.

Conflicts of interest

There are no conflicts to declare.

Acknowledgements

The authors acknowledge the computational support from ARCHER2, CENAPAD-SP, and CCCT-CP at UTFPR-CP.

Notes and references

1 N. G. Loeb, G. C. Johnson, T. J. Thorsen, J. M. Lyman, F. G. Rose and S. Kato, *Geophys. Res. Lett.*, 2021, **48**, e2021GL093047.
2 M. T. Richardson, *Geophys. Res. Lett.*, 2022, **49**, e2021GL095782.
3 G. Li, M. Li, R. Taylor, Y. Hao, G. Besagni and C. N. Markides, *Appl. Therm. Eng.*, 2022, **209**, 118285.
4 A. Rahman, O. Farrok and M. M. Haque, *Renewable Sustainable Energy Rev.*, 2022, **161**, 112279.
5 M. Younas, S. Shafique, A. Hafeez, F. Javed and F. Rehman, *Fuel*, 2022, **316**, 123317.
6 S. P. S. Badwal, S. Giddey, A. Kulkarni, J. Goel and S. Basu, *Appl. Energy*, 2015, **145**, 80–103.
7 J. Goldemberg, *Science*, 2007, **315**, 808–810.
8 L. Yaqoob, T. Noor and N. Iqbal, *RSC Adv.*, 2021, **11**, 16768–16804.
9 L. An, T. S. Zhao, X. L. Zhou, L. Wei and X. H. Yan, *RSC Adv.*, 2014, **4**, 65031–65034.
10 L. An, T. Zhao and Y. Li, *Renewable Sustainable Energy Rev.*, 2015, **50**, 1462–1468.
11 C.-L. Sun, J.-S. Tang, N. Brazeau, J.-J. Wu, S. Ntais, C.-W. Yin, H.-L. Chou and E. A. Baranova, *Electrochim. Acta*, 2015, **162**, 282–289.
12 A. B. D. M. Jacquot, M. Chatenet and C. Cremers, *Phys. Chem. Chem. Phys.*, 2016, **18**, 25169–25175.
13 K. Rossi, G. G. Asara and F. Baletto, *ACS Catal.*, 2020, **10**, 3911–3920.
14 K. Rossi, G. G. Asara and F. Baletto, *ChemPhysChem*, 2019, **19**, 3037–3044.
15 F. Baletto, *J. Phys.: Condens. Matter*, 2019, 113001.
16 V. A. Rigo, C. R. Miranda and F. Baletto, *Eur. Phys. J. B*, 2019, **92**, 1.
17 C. Li, K. Wang and D. Xie, *Surf. Interfaces*, 2022, **28**, 101594.
18 L. G. Verga, J. Aarons, M. Sarwar, D. Thompsett, A. Russell and C.-K. Skylaris, *Phys. Chem. Chem. Phys.*, 2016, **18**, 32713–32722.
19 L. G. Verga, A. E. Russell and C.-K. Skylaris, *Phys. Chem. Chem. Phys.*, 2018, **20**, 25918–25930.
20 J. Perez, V. A. Paganin and E. Antolini, *J. Electroanal. Chem.*, 2011, **654**, 108–115.
21 P. Hohenberg and W. Kohn, *Phys. Rev.*, 1964, **136**, B864.
22 W. Kohn and L. J. Sham, *Phys. Rev.*, 1965, **140**, A1133.
23 P. Giannozzi, S. Baroni, N. Bonini, M. Calandra, R. Car, C. Cavazzoni, D. Ceresoli, G. L. Chiarotti, M. Cococcioni, I. Dabo, A. D. Corso, S. de Gironcoli, S. Fabris, G. Fratesi, R. Gebauer, U. Gerstmann, C. Gougoussis, A. Kokalj, M. Lazzeri, L. Martin-Samos, N. Marzari, F. Mauri, R. Mazzarello, S. Paolini, A. Pasquarello, L. Paulatto, C. Sbraccia, S. Scandolo, G. Sclauzero, A. P. Seitsonen, A. Smogunov, P. Umari and R. M. Wentzcovitch, *J. Phys.: Condens. Matter*, 2009, **21**, 395502.

 This journal is © the Owner Societies 2023

Published on 09 January 2023. Downloaded on 4/7/2026 5:10:41 AM.

24 P. Giannozzi, O. Andreussi, T. Brumme, O. Bunau, M. B. Nardelli, M. Calandra, R. Car, C. Cavazzoni, D. Ceresoli, M. Cococcioni, N. Colonna, I. Carnimeo, A. D. Corso, S. de Gironcoli, P. Delugas, R. A. DiStasio, A. Ferretti, A. Floris, G. Fratesi, G. Fugallo, R. Gebauer, U. Gerstmann, F. Giustino, T. Gorni, J. Jia, M. Kawamura, H.-Y. Ko, A. Kokalj, E. Küçükbenli, M. Lazzeri, M. Marsili, N. Marzari, F. Mauri, N. L. Nguyen, H.-V. Nguyen, A. O. de-la Roza, L. Paulatto, S. Poncé, D. Rocca, R. Sabatini, B. Santra, M. Schlipf, A. P. Seitsonen, A. Smogunov, I. Timrov, T. Thonhauser, P. Umari, N. Vast, X. Wu and S. Baroni, *J. Phys.: Condens. Matter*, 2017, **29**, 465901.
25 J. P. Perdew, K. Burke and M. Ernzerhof, *Phys. Rev. Lett.*, 1996, **77**, 3865–3868.
26 D. Vanderbilt, *Phys. Rev. B: Condens. Matter Mater. Phys.*, 1990, **41**, 7892–7895.
27 S. Grimme, J. Antony, S. Ehrlich and H. Krieg, *J. Chem. Phys.*, 2010, **132**, 154104.
28 S. R. Billeter, A. J. Turner and W. Thiel, *Phys. Chem. Chem. Phys.*, 2000, **2**, 2177–2186.
29 S. R. Billeter, A. Curioni and W. Andreoni, *Comput. Mater. Sci.*, 2003, **27**, 437–445.
30 P.-O. Löwdin, *J. Chem. Phys.*, 1950, **18**, 365–375.
31 L. D. Marks, *J. Cryst. Growth*, 1983, **61**, 556–566.
32 F. Baletto, C. R. Miranda, V. A. Rigo and K. Rossi, Nanoalloys for energy applications, in *Nanoalloys*, ed. F. Calvo, Elsevier, Oxford, 2nd edn, 2020, pp. 347–380.
33 T.-K. Yeh and C.-H. Chen, *J. Power Sources*, 2008, **184**, 353–362.
34 C. Hu, Y. Zhou, M. Xiao and G. Yu, *Int. J. Hydrogen Energy*, 2020, **45**, 4341–4354.
35 A. von Weber and S. L. Anderson, *Acc. Chem. Res.*, 2016, **49**, 2632–2639.
36 Y. Ma, C. Ricciuti, T. Miller, J. Kadlowec and H. Pearlman, *Energy Fuels*, 2008, **22**, 3695–3700.
37 J. L. C. Fajín, A. Bruix, M. N. D. S. Cordeiro, J. R. B. Gomes and F. Illas, *J. Chem. Phys.*, 2012, **137**, 034701.
38 A. O. Pereira and C. R. Miranda, *Appl. Surf. Sci.*, 2014, **288**, 564–571.
39 P. Tereshchuk and J. L. F. Da Silva, *J. Phys. Chem. C*, 2012, **116**, 24695–24705.
40 R. L. H. Freire, A. Kiejnab and J. L. F. Da Silva, *Phys. Chem. Chem. Phys.*, 2016, **18**, 29526–29536.
41 L. Zibordi-Besse, P. Tereshchuk, A. S. Chaves and J. L. F. Da Silva, *J. Phys. Chem. A*, 2016, **120**, 4231–4240.
42 C. G. Broyden, J. E. J. Dennis and J. J. Moré, *J. Inst. Maths. Appl.*, 1973, **12**, 223–245.
43 G. Henkelman and H. Jónsson, *J. Chem. Phys.*, 1999, **111**, 7010.
44 A. Sapi, F. Liu, X. Cai, C. M. Thompson, H. Wang, K. An, J. M. Krier and G. A. Somorjai, *Nano Lett.*, 2014, **14**, 6727–6730.
45 H.-F. Wang and Z.-P. Liu, *J. Am. Chem. Soc.*, 2008, **130**, 10996–11004.
46 Z.-d Wang, Y. Gan, Y.-l Mai, Y. Shi, S. Cao, Z.-x Lu, C.-q Guo, H. Tan and C.-f Yan, *Anal. Chem.*, 2020, **92**, 8046–8050.
47 C. Hu, Y. Zhou, M. Xiao and G. Yu, *Int. J. Hydrogen Energy*, 2020, **45**, 4341–4354.